

Superlattice nanowire heat engines with direction-dependent power output and heat current

David M T Kuo¹, and Yia-Chung Chang^{2,3}

¹*Department of Electrical Engineering and Department of Physics,
National Central University, Chungli, 320 Taiwan*

²*Research Center for Applied Sciences, Academic Sinica, Taipei, 11529 Taiwan and*

³*Department of Physics, National Cheng Kung University, Tainan, 701 Taiwan*

(Dated: March 18, 2022)

Heat engines (HEs) made of low dimensional structures offer promising applications in energy harvesting due to their reduced phonon thermal conductance. Many efforts have been devoted to the design of HEs made of quantum-dot (QD) superlattice nanowire (SLNW), but only SLNWs with uniform energy levels in QDs were considered. Here we propose a HE made of SLNW with staircase-like QD energy levels. It is demonstrated that the nonlinear Seebeck effect can lead to significant electron transports for such a nanowire with staircase-like energy levels. The asymmetrical alignment of energy levels of quantum dots embedded in nanowires can be controlled to allow resonant electron transport under forward temperature bias, while they are in off-resonant regime under backward bias. Under such a mechanism, the power output and efficiency of such a SLNW are better than SLNWs with uniform QD energy levels. The SLNW HE has direction-dependent power output and heat current. In addition, the HE has the functionality of a heat diode with impressive negative differential thermal conductance under open circuit condition.

1. Introduction

Recently, many efforts were devoted to the studies of the nonlinear thermoelectric properties of low dimension systems for the applications of energy harvesting.[1-13] The figure of merit (ZT) of quantum dots (QDs) junction system may approach infinity (corresponding to Carnot efficiency) in the weak coupling between QD and electrodes when systems have a vanishingly small phonon thermal conductance.[14] However, their electrical power output is extremely weak due to very small electron tunneling rates.[1,14] A remarkable thermoelectric device needs not only a high efficiency but also significant power output.[5,6] Therefore, how to design a heat engine with near Carnot efficiency and optimized power output is under hot pursuit.[7-13] QD superlattice nanowires (SLNWs) offer high potential to realize significantly reduced phonon thermal conductance.[15,16] It is expected that the efficiency of SLNW heat engines (HEs) is relatively high when compared with other low dimensional systems. Nevertheless, theoretical studies of SLNW HEs reported so far are based on the assumption of uniform energy levels in QDs without considering the effect of nonlinear Seebeck voltage resulting from temperature bias.[5,8,17]

Most recently, Ref.[18] has pointed out that nonlinear Seebeck voltage plays a remarkable role for heat diode design by considering hetero-molecular junctions. Therefore, we attempt to reveal the effect of Seebeck voltage on the power output and TE efficiency of SLNW HEs. Furthermore, we also demonstrate that electron heat diodes can be implemented by using nonlinear Seebeck voltage of a QD SLNW with staircase-like energy levels. The design structure is shown in Fig. 1. Although the staircase-like energy levels of QDs in a SLNW make it difficult for the electron transport under a small temperature bias, a suitable alignment of QD energy levels

can be designed to allow resonant electron transport under large forward temperature bias, while the system is in off-resonant regime under backward bias. This mechanism can give rise to a high efficiency and optimized power output for SLNW HEs.

2. Theoretical method

To study the direction-dependent nonlinear thermoelectric properties of QD SLNW connected to metallic electrodes shown in Fig. 1(a), we start with the system Hamiltonian given by an extended Anderson model $H = H_0 + H_{QD}$ [19,20], where

$$H_0 = \sum_{k,\sigma} \epsilon_k a_{k,\sigma}^\dagger a_{k,\sigma} + \sum_{k,\sigma} \epsilon_k b_{k,\sigma}^\dagger b_{k,\sigma} \quad (1)$$

$$+ \sum_{k,s} V_{k,L}^L d_{L,s}^\dagger a_{k,\sigma} + \sum_{k,s} V_{k,R}^R d_{R,s}^\dagger b_{k,\sigma} + c.c.$$

The first two terms of Eq. (1) are for free electrons in the left and right electrodes. $a_{k,\sigma}^\dagger$ ($b_{k,\sigma}^\dagger$) creates an electron of momentum k and spin σ with energy ϵ_k in the left (right) electrode. $V_{k,L}^L$ ($V_{k,R}^R$) describes the coupling between the leftmost (rightmost) QD in the SLNW and the left (right) electrode. $d_{L(R),s}^\dagger$ ($d_{L(R),s}$) creates (destroys) an electron in the leftmost (rightmost) QD. s labels the degenerate states in a QD level with orbital and spin degeneracy.[21] Silicon has six equivalent valleys, each having an ellipsoidal shape. In a SLNW with strong lateral confinement along x and y directions, the energy of electron states in two valleys elongated along the z axis will be lifted up more than electronic states in the remaining four valleys. Thus, we consider the four-fold valley degeneracy for each QD.

$$H_{QD} = \sum_{\ell,s} E_\ell n_{\ell,s} + \sum_{\ell \neq j} t_{\ell,j} d_{\ell,s}^\dagger d_{j,s} + c.c. \quad (2)$$

where E_ℓ denotes the energy of the level of the ℓ -th QD, and $t_{\ell,j}$ describes the electron hopping strength between the ℓ -th QD and its nearest neighbor QD labeled by j . For the SLNW depicted in Fig. 1(a), E_ℓ depends on the location of QD. Here, we assume the QD energy levels have a staircase-like distribution as shown in Fig. 1(b) in which $E_N = E_R$, and $E_\ell = E_R + (N - \ell)\Delta E$, where ΔE denotes the energy level separation. Such a variation in QD levels can be engineered by considering suitable diameter variation of QDs in the SLNW shown in Fig. 1(a), which can be realized by the advanced etch and lithography technique[15,17]. The electron Coulomb interactions have been neglected in Eq. (2). The electron Coulomb interactions are weak under the resonant tunneling condition, since the electron wavefunction in SLNW becomes delocalized. Although intra and inter-dot electron Coulomb interactions are strong in the off-resonant condition, the effect of electron Coulomb interactions on the electron transport becomes small when the electron population of each QD is small.[21]. This study is restricted in this situation.

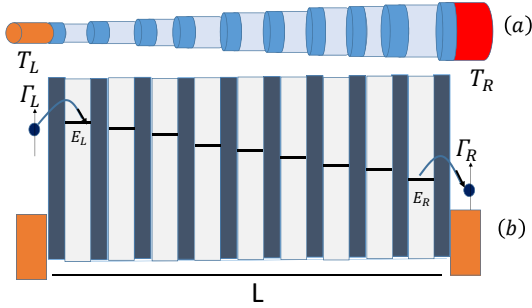


FIG. 1: (a) Schematic illustration of heat engine made of quantum dots embedded in a nanowire with length L connected to metallic electrodes. (b) Energy diagram illustrating a QD array with staircase-like alignment of energy levels connected to metallic electrodes at $T_L = T_R$, where T_L and T_R are the equilibrium temperature of left and right electrodes. Γ_L (Γ_R) denote the tunneling rates for electrons from the left (right) electrode entering the leftmost (rightmost) QD with energy level E_L (E_R).

The electron current from electrode to the QD SLNW can be derived by using the Meir-Wingreen formula.[20] We have

$$J = \frac{se}{\hbar} \int \frac{d\epsilon}{2\pi} \mathcal{T}_{LR}(\epsilon) [f_L(\epsilon) - f_R(\epsilon)], \quad (3)$$

where $f_\alpha(\epsilon) = 1/\{\exp[(\epsilon - \mu_\alpha)/k_B T_\alpha] + 1\}$ denotes the Fermi distribution function for the α -th electrode, where μ_α and T_α are the chemical potential and the temperature of the α electrode. e , \hbar , and k_B denote the electron charge, the Planck's constant, and the Boltzmann

constant, respectively. $\mathcal{T}_{LR}(\epsilon)$ denotes the transmission coefficient of QD SLNW connected to electrodes, which can be derived by the equation of motion method.[22]

The expression of transmission coefficient is given by

$$\mathcal{T}_{L,R}(\epsilon) = \frac{4\Gamma_L(\epsilon)\Gamma_R^{eff}(\epsilon)}{\Gamma_L(\epsilon) + \Gamma_R^{eff}(\epsilon)} (-Im(G_L^r(\epsilon))), \quad (4)$$

where the tunneling rate $\Gamma_{L(R)}(\epsilon) = 2\pi \sum_k |V_{k,L(R)}|^2 \delta(\epsilon - \epsilon_k)$. In the wide band limit of electrodes, the energy-dependent $\Gamma_{L(R)}(\epsilon)$ can be neglected. The notation Im means taking the imaginary part of the function that follows, and

$$G_L^r(\epsilon) = 1/(\epsilon - E_1 + i\Gamma_L - \Sigma_{1,N}) \quad (5)$$

is the one-particle retarded Green function of the leftmost QD with the energy level of E_1 . The self energy $\Sigma_{1,N}(\epsilon)$ results from electron tunneling from the leftmost QD to the right electrode mediated by $N-1$ QDs, which is given by [17,22]

$$\Sigma_{1,N} = \frac{t_{1,2}^2}{\epsilon - E_2 - \frac{t_{2,3}^2}{\epsilon - E_3 - \dots - \frac{t_{N-1,N}^2}{\epsilon - E_N + i\Gamma_R}}}, \quad (6)$$

where N denotes the total number of QDs. The rightmost QD is the N th QD. The effective tunneling rate $\Gamma_R^{eff}(\epsilon) = -Im(\Sigma_{1,N}(\epsilon))$. For simplicity, we assume $t_{\ell,j} = t_c$ for all ℓ and j being the nearest neighbor of ℓ , and $\Gamma_L = \Gamma_R = \Gamma$. Note that $\mathcal{T}_{LR}(\epsilon)$ of QD chain can also be found in early work[23], where authors calculated the Green's function in terms of matrix form.

The heat current for electrons leaving from the left (right) electrode is given by[22]

$$Q_{e,L(R)} = \frac{\pm s}{\hbar} \int \frac{d\epsilon}{2\pi} \mathcal{T}_{LR}(\epsilon) (\epsilon - \mu_{L(R)}) [f_L(\epsilon) - f_R(\epsilon)]. \quad (7)$$

We note that $Q_{e,L} + Q_{e,R} = -(\mu_L - \mu_R)J/e$, which describes the Joule heating.

Because the phonon heat current (Q_{ph}) coexists with the electron heat current, we should examine how Q_{ph} will influence the efficiency of a SLNW HE. To include Q_{ph} we adopted the following empirical formula given in Ref.[24]

$$Q_{ph}(T) = \frac{F_s}{\hbar} \int \frac{d\omega}{2\pi} \mathcal{T}_{ph}(\omega) (\hbar^2 \omega) [n_L(\omega) - n_R(\omega)], \quad (8)$$

where ω and $\mathcal{T}_{ph}(\omega)$ are the phonon frequency and throughput function, respectively. $\mathcal{T}_{ph}(\omega)$ depends on the length (L), surface roughness width (δ) and diameter (D) of silicon nanowires.[24] $n_{L(R)} = 1/(\exp(\hbar\omega/k_B T_{L(R)}) + 1)$. In the linear response region, $Q_{ph} = \kappa_{ph} \Delta T$, where κ_{ph} and ΔT are the phonon thermal conductance and temperature difference between electrodes. In Ref.[24],

theoretical κ_{ph} illustrates the experimental κ_{ph} of silicon nanowires below 300K very well. Because authors have not considered the phonon-phonon collisions in silicon nanowires, Eq. (8) is not adequate to describe Q_{ph} in high temperature region of $T > 300K$. A dimensionless factor F_s is introduced to describe the reduction factor for phonon transport due to scattering from QDs embedded in a nanowire.[25] The value of $F_s = 0.1$ is used throughout this article, which is determined according to Ref.[25], in which the phonon thermal conductance of silicon/germanium QD SLNWs is calculated. Due to the low electron density considered here and weak electron phonon interactions (EPI) in Si/Ge, the electron mean free path (λ) of Si/Ge QD SLNWs is longer than 170 nm at room temperature. The length of QD SLNW considered here is around 127 nm, which is smaller than λ reported in Ref.[26]. Therefore, the neglect of EPIs is justified.

To design a heat engine driven by a high temperature-bias $\Delta T = T_L - T_R$, the Seebeck voltage ($eV_{th} = \mu_L - \mu_R$) across the external load with conductance $G_{ext} = 1/R_{ext}$ needs to be calculated.[12] Meanwhile, the energy levels E_ℓ for all ℓ should be readjusted according to V_{th} . As a consequence, $\mathcal{T}_{LR}(\epsilon)$ will depend on V_{th} . The electron heat current satisfies the condition $Q_{e,L} + Q_{e,R} = -JV_{th} = P_{gen}$, which denotes the work done by the heat engine per unit time. The efficiency of heat engine is defined as the power output divided by the power input. The power input is the heat current out of the hot side and the power output is the electrical power generated P_{gen} . Thus, the direction-dependent efficiency of heat engine is given by

$$\eta_\alpha = -JV_{th}/|Q_{e,\alpha}|. \quad (9)$$

We define $\Delta T > 0$ and $\Delta T < 0$ as the forward temperature bias and backward temperature bias. When $\Delta T > 0$ ($\Delta T < 0$), the electron heat current is leaving from the left (right) electrode, $Q_{e,\alpha}$ in Eq. (9) denotes the $Q_{e,L}$ ($Q_{e,R}$) in Eq. (7).

3. Results and discussion

We consider an $N = 25$ SLNW with a staircase alignment of energy levels. Namely, we have $E_L = E_1 = E_R + 24\Delta E$, $E_2 = E_R + 23\Delta E \dots$ and $E_N = E_R$. With an induced Seebeck voltage, V_{th} , the energy levels E_ℓ are modified according to $\varepsilon_\ell = E_\ell + \eta_\ell eV_{th}$. In a simple approximation where the electric field is uniformly distributed in spacer layers in the SLNW, the level modulation factor is expressed as $\eta_\ell = -(\ell L_s - L/2)/L$ with $\mu_{L(R)} = E_F \pm eV_{th}/2$. The pair length (that of one QD plus one spacer layer) adopted is $L_s = 5$ nm and the length of SLNW is $L = 127$ nm.[25] The Seebeck voltage can be evaluated by Eq. (3) under the condition of $G_{ext}V_{th} + J(V_{th}, \Delta T) = 0$, which is the same as the experimental configuration in Ref [12], where authors studied the HE made of a single QD connected to electrodes. Once V_{th} is obtained, the electron current J and electron heat current $Q_{e,L(R)}$ can be evaluated by Eq.(3) and Eq. (7), respectively. The resulting output power,

P_{gen} and V_{th} as functions of temperature bias for various values of ΔE at $t_c = \Gamma_L = \Gamma_R = 1\Gamma_0$, $G_{ext} = 0.04G_0$ and $E_R = E_F + 4\Gamma_0$ are plotted in Fig. 2. $G_0 = e^2/h$ denotes the quantum conductance and E_F is the Fermi energy of electrodes. All energy scales are in units of Γ_0 throughout this article. The value of Γ_0 depends on the desired temperature range considered in the design. In typical designs considered, $\Gamma_0 = 1$ meV

Figure 2(a) shows the asymmetrical behavior of output power, P_{gen} . It is found that P_{gen} under backward temperature bias ($\Delta T < 0$) is always smaller than that under forward bias ($\Delta T > 0$). The asymmetry ratio, $R_{asy} = P_{gen}(1\Gamma_0)/P_{gen}(-1\Gamma_0)$ is found to be 1, 1.43, and 2.81 for $\Delta E = 0, 0.05\Gamma_0$, and $0.1\Gamma_0$, respectively. Such a ratio is enhanced with increasing ΔT . To understand the asymmetrical behavior of P_{gen} , it is important to examine the relation between V_{th} and ΔT . (See Fig. 2(b)) Non-linear Seebeck coefficients ($V_{th}/\Delta T$) are always negative, indicating that electrons of the electrodes mainly diffuse through energy levels above E_F . The Seebeck voltage not only changes chemical potentials of electrodes ($\mu_{L(R)} = E_F \pm eV_{th}/2$), which counter balances the electron flow from the hot side to the cold side, but also influences the alignment of energy levels. With forward temperature bias, the QD levels are tilted toward alignment, allowing resonant tunneling of electrons from the left electrode to the right electrode, while under reverse bias the QD levels are further misaligned, leading to an off-resonance condition. (See insets in Fig. 2(a)) In the limit of $\Delta T \rightarrow 0$, we have $G_{ext}V_{th} + e^2\mathcal{L}_0V_{th} + \mathcal{L}_1\frac{\Delta T}{eT} = 0$, where $\mathcal{L}_n = \frac{s}{h} \int d\epsilon \mathcal{T}_{LR}(\epsilon)(\epsilon - E_F)^n \frac{1}{4k_B T \cosh^2((\epsilon - E_F)/(2k_B T))}$ with $s = 8$ resulting from the four-fold valley degeneracy and spin. Note that transmission coefficient $\mathcal{T}_{LR}(\epsilon)$ in \mathcal{L}_n is independent of V_{th} . The Seebeck voltage is then given by $V_{th} = \frac{-\mathcal{L}_1\Delta T}{(eT)(G_{ext} + e^2\mathcal{L}_0)}$, which explains that V_{th} and ΔT always have opposite signs, if $E_R > E_F$ and P_{gen} is proportional to ΔT^2 . In the nonlinear response region, $\mathcal{T}_{LR}(\epsilon)$ involves V_{th} , the relation between V_{th} and ΔT can be rather complicated.

Because $P_{gen}(\Delta T > 0)$ is larger than $P_{gen}(\Delta T < 0)$ in Fig. 2(a), we further investigate the electron heat current $Q_{e,L}$ and efficiency η as functions of forward temperature bias in Fig. 3(a) and 3(b), respectively. Like P_{gen} , the electron heat current $Q_{e,L}$ at $\Delta E = 0$ is smaller than that at $\Delta E = 0.1\Gamma_0$. In particular, the maximum efficiency of HEs (η_{max}) at $\Delta E = 0.1\Gamma_0$ is better than the case of $\Delta E = 0$. The $\eta_{max} = 0.75$ for $\Delta E = 0.1\Gamma_0$ corresponds to ZT larger than fifteen according to $\eta/\eta_c = (\sqrt{ZT+1}-1)/(\sqrt{ZT+1}+1)$. [16] From the results of Fig. 2(a) and Fig. 3(b), we have demonstrated that the P_{gen} and η of SLNW HEs with staircase-like energy levels have better performance. Fig. 3(c) shows the dependence of η on the external load resistance, R_{ext} . The R_{ext} -dependent η has been investigated in the experiment of Ref.[12] The dotted curve includes the phonon heat current Q_{ph} , where a silicon nanowire with surface roughness width $\delta = 3$ nm, diameter $D = 3$ nm and $L = 127$ nm is considered. The behavior of $Q_{ph}(T, \Delta T)$ was reported

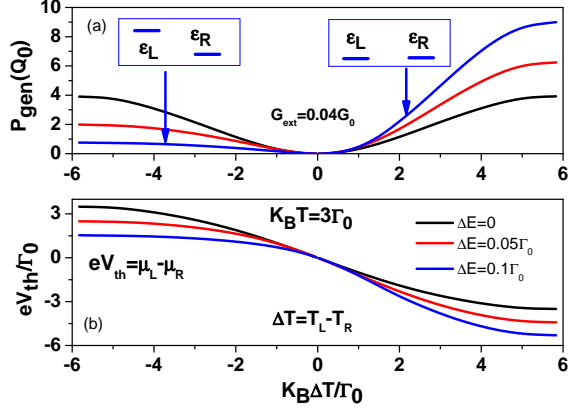


FIG. 2: (a) Electrical power output, (b) Seebeck-voltage as functions of temperature bias for different ΔE values at $T = 36K$, $E_R = E_F + 4\Gamma_0$, $t_{\ell,j} = t_c = 1\Gamma_0$ and $\Gamma_L = \Gamma_R = \Gamma = 1\Gamma_0$. $Q_0 = \Gamma_0^2/h$. $T_L = T + \Delta T/2$ and $T_R = T - \Delta T/2$.

for different diameters of silicon nanowires in our previous work [27]. The suppression of $\eta = P_{gen}/(Q_{e,L} + Q_{ph})$ due to finite Q_{ph} is expected. The maximum η occurs at $R_{ext} \approx 20R_0$, where $R_0 = 1/G_0$. Note that when $R_{ext} \rightarrow 0$, we have $V_{th} \rightarrow 0$, which leads to vanishingly small P_{gen} . On the other hand, as $R_{ext} \rightarrow \infty$ we have $J \rightarrow 0$ and $P_{gen} \rightarrow 0$. Fig. 3(d) shows η as a function of E_R at $\Delta E = 0.1\Gamma_0$. The maximum η occurs near $E_R = E_F + 5\Gamma_0$. In this case, all QD energy levels are above E_F , and the electron transport is mainly due to thermionic process.

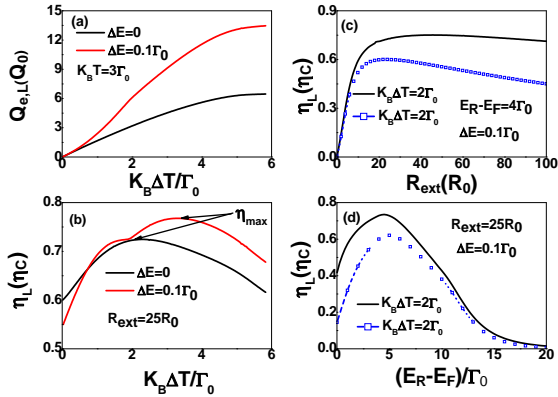


FIG. 3: (a) Electron heat current Q_L and (b) efficiency η_L as functions of temperature bias for different ΔE values at $K_B T = 3\Gamma_0$ and $E_R = E_F + 4\Gamma_0$. (c) η_L as functions of R_{ext} at $K_B \Delta T = 2\Gamma_0$, $\Delta E = 0.1\Gamma_0$, $K_B T = 3\Gamma_0$ and $E_R = E_F + 4\Gamma_0$. (d) η_L as functions of E_R at $K_B \Delta T = 2\Gamma_0$, $\Delta E = 0.1\Gamma_0$, $K_B T = 3\Gamma_0$ and $R_{ext} = 25R_0$. $R_0 = 1/G_0$. Other physical parameters are $t_c = \Gamma = 1\Gamma_0$, $\eta_c = \Delta T/T_L$.

Heat diodes (HDs) play an important role in applications of energy harvesting [28–34]. Those designs consid-

ered three kinds of heat carriers: phonons,[28–30], photons [31], and electrons [18,27]. To investigate the behavior of SLNW HDs, we consider the open-circuit condition of $J = 0$ [18,27] that $Q_{e,L} = -Q_{e,R} = Q_e$ in which the contribution involving $\mu_{L(R)}$ is zero in Eq. (7). The rectification ratio of HDs is defined as $R_r = \frac{Q_e(\Delta T > 0)}{|Q_e(\Delta T < 0)|}$, where $Q_e(\Delta T > 0)$ and $Q_e(\Delta T < 0)$ are the heat currents in the forward and backward temperature bias, respectively. Fig. 4(a) shows the calculated electron heat current as a function of temperature bias, and the behavior of the direction-dependent electron heat current (heat rectification) is apparent. Note that Q_e is not zero although $J = 0$. Under forward bias, a negative differential thermal conductance (NDTC) is observed. To analyze the behavior of NDTC, we examine the Seebeck voltage (V_{th}) as a function of ΔT in Fig. 4(b). For simplicity, let's consider $t_c = 2\Gamma_0$, which corresponds to a narrow bandwidth case. For this case, the QD energy levels are aligned (the resonant-tunneling condition) when $K_B \Delta T = 2.5\Gamma_0$, which corresponds to $eV_{th} = -10\Gamma_0$ for $\Delta E = 0.4\Gamma_0$. When $K_B \Delta T$ deviates from $2.5\Gamma_0$, the system is driven away from the resonant condition. This explains why the electron heat current has a peak near $K_B \Delta T = 2.5\Gamma_0$, which leads to NDTC as $K_B \Delta T$ exceeds $2.5\Gamma_0$. In Fig. 4(c), we show the electron heat rectification ratio (R_r) as a function of ΔT . Although the maximum R_r reaches a very high value near 60 at $t_c = 2\Gamma_0$, the heat current is very small. Good thermal diodes also require large heat current. Thus, the cases with $t_c = 3\Gamma_0$ (red) and $4\Gamma_0$ (blue) are better designs than the $t_c = 2\Gamma_0$ case, since the heat current is significantly higher even though the maximum R_r is somewhat lower. The differential thermal conductances (DTC) corresponding to the curves shown in Fig. 4(a) are given in Fig. 4(d) in which very robust NDTC behavior is observed. The feature of NDTC plays a remarkable role in the design of thermal transistors.[32–34] So far, little literature has reported NDTC resulting from electron carriers. It is worth noting that the study of Ref.[18] does not show the NDTC behavior for hetero-molecular junction, this may be attributed to $\Delta T/T$ not large enough. According to the results of Fig. 4, the ratio of $\Delta T/T > 1$ is preferred to observe the feature of NDTC.

For further optimization we calculate Q_e and R_r as functions of ΔT for various values of E_R at $t_c = \Gamma_L = \Gamma_R = 4\Gamma_0$, $K_B T = 3\Gamma_0$, and $\Delta E = 0.4\Gamma_0$. The results are shown in Fig. 5. At a given value of positive ΔT , $Q_e(\Delta T > 0)$ is suppressed with increasing E_R due to the reduction of electron population at high energy levels in the thermionic process. In the thermal-assisted transport process, V_{th} increases significantly with increasing E_R (not shown). In the cases of $E_R = E_F + 4\Gamma_0$ and $E_R = E_F + 6\Gamma_0$, the magnitude of V_{th} is not enough to create the resonant-tunneling condition for electron transport under forward bias. Therefore, no NDTC is observed in these two cases. In Fig. 5(b), it is seen that η_R for $E_R = E_F + 4\Gamma_0$ reaches a very impressive value of 100. However, the maximum η_R for this case is reduced to near

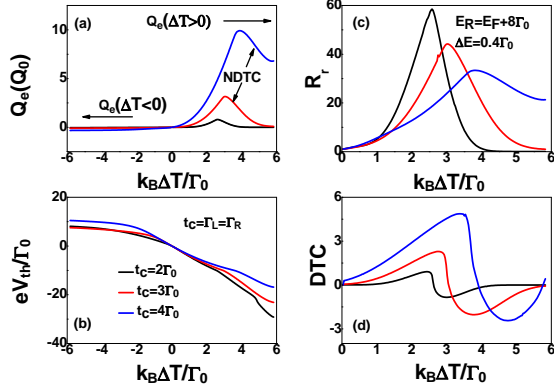


FIG. 4: (a) Electron heat current Q_e , (b) Seebeck voltage V_{th} , (c) heat rectification ratio η_R and (d) differential thermal conductance (DTC) as functions of temperature bias for different electron hopping strengths. $G_{ext} = 0$, $t_c = \Gamma_L = \Gamma_R$, $K_B T = 3 \Gamma_0$ and $E_R = E_F + 8 \Gamma_0$.

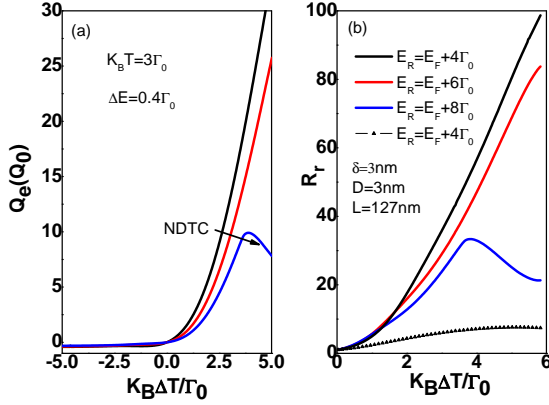


FIG. 5: (a) Electron heat current Q_e , and (b) heat rectification ratio as functions of temperature bias for different E_R values at $t_c = \Gamma_L = \Gamma_R = 4 \Gamma_0$, $K_B T = 3 \Gamma_0$, and $\Delta E = 0.4 \Gamma_0$.

10 when Q_{ph} is included (dotted curve). In the design of semiconductor HDs with high R_r values, obviously, the reduction of Q_{ph} is strongly required. It is expected that the effect of phonon heat current can be reduced in the future with the advances in nanotechnology [25]. Therefore, the HEs and HDs of SLNW with staircase-like QD energy levels exist the promising potential in the applications of energy harvesting.

4. Summary

In conclusion, we have theoretically investigated the direction-dependent electrical power output and electron heat rectification of a QD SLNW. The alignment of energy levels of QDs in the nanowire can be altered by the temperature-bias induced Seebeck voltage which leads to resonant tunneling for electrons in forward bias but off-resonance in reverse bias for properly designed distribution of QD energy levels in SLNW. This provides a physical mechanism for achieving direction-dependent P_{gen} and Q_e . We found that the maximum efficiency and optimized P_{gen} of SLNW with staircase-like QD energy levels are better than those of SLNW with uniform QD energy levels. In addition, we have demonstrated that such SLNWs have unique behavior not only in electron heat rectification but also in NDTC, which is a key ingredient for the implementation of thermal logical gates and transistors.

Acknowledgments

This work was supported by the Ministry of Science and Technology (MOST) of Taiwan under contract nos. 107-2112-M-008-023-MY2 and 107-2112-M-001-032.

¹E-mail address: mtkuo@ee.ncu.edu.tw

²E-mail address: yiachang@gate.sinica.edu.tw

¹ D. M. T. Kuo and Y. C. Chang, Phys. Rev. B **81**, 205321 (2010).
² N. Nakpathomkun, H. Q. Xu and H. Linke, Phys. Rev. B **82**, 235428 (2010).
³ M. Leijnse, M. R. Wegewijs and K. Flensberg, Phys. Rev. B **82**, 045412 (2010).
⁴ A. N. Jordan, B. Sothmann, R. Sanchez, M. Buttiker, Phys. Rev. B, **87**, 075312 (2013).
⁵ R. S. Whitney, Phys. Rev. Lett. **112**, 130601 (2014).
⁶ R. S. Whitney, Phys. Rev. B **91**, 115425 (2015).
⁷ F. Hartmann, P. Pfeffer, S. Höffling, M. Kamp, and L. Worschech, Phys. Rev. Lett. **114**, 146805 (2015).
⁸ H. Karbaschi, J. Loven, K. Courteaut, A. Wacker, and M. Leijnse, Phys. Rev. B **94**, 115414 (2016).
⁹ B. De and B. Muralidharan, Phys. Rev. B **94**, 165416

(2016).
¹⁰ A. M. Dare and P. Lombardo, Phys. Rev. B, **96**, 115414 (2017).
¹¹ P. A. Erdman, F. Mazza, R. Bosisio, G. Benenti, R. Fazio, and F. Taddei, Phys. Rev. B **95**, 245432 (2017).
¹² M. Josefsson, A. Svilans, A. M. Burke, E. A. Hoffmann, S. Fahlvik, C. Thelander, M. Leijnse and H. Linke, Nature Nanotechnology, **13**, 920 (2018).
¹³ P. Pietzonka and Udo Seifert, Phys. Rev. Lett. **120**, 190602 (2018).
¹⁴ P. Murphy, S. Mukerjee, and J. Moore, Phys. Rev. B **78**, 161406(R) (2008).
¹⁵ T. C. Harman, P. J. Taylor, M. P. Walsh, B. E. LaForge, Science **297**, 2229 (2002).
¹⁶ M. Zebbarjadi, K. Esfarjania, M.S. Dresselhaus, Z.F. Ren

- and G. Chen, *Energy Environ Sci* **5**, 5147 (2012).
- ¹⁷ D. M.-T. Kuo, C. C. Chen, and Y.-C. Chang, *Physica E* **102**, 39 (2018).
 - ¹⁸ G. T. Craven, D. H. He and A. Nitzan, *Phys. Rev. Lett.* **121**, 247704 (2018).
 - ¹⁹ H. Haug and A. P. Jauho, *Quantum Kinetics in Transport and Optics of Semiconductors* (Springer, Heidelberg, 1996).
 - ²⁰ A. P. Jauho, N. S. Wingreen and Y. Meir, *Phys. Rev. B* **50**, 5528 (1994), and references therein.
 - ²¹ David M T Kuo, C. C. Chen and Y. C. Chang, *Phy. Rev. B* **95**, 075432 (2017).
 - ²² D. M. T. Kuo, S. Y. Shiao and Y. C. Chang, *Phys. Rev. B.* **84**, 245303 (2011).
 - ²³ B.H. Teng, H. Sy, Z.Wang, Y. Sun, and H. Yang, *Phys. Rev. B* **75** 012105 (2007).
 - ²⁴ R. K. Chen, A. I. Hochbaum, P. Murphy, J. Moore, P. D. Yang, and A. Majumdar, *Phys. Rev. Lett.* **101**, 105501 (2008).
 - ²⁵ M. Hu and D. Poulikakos, *Nano Lett.* **12**, 5487 (2012).
 - ²⁶ W. Lu, J. Xiang, B. P. Timko, Y. Wu, C. M. Lieber, *Proc. Natl. Acad. Sci. U.S. A.* **102**, 10046 (2005).
 - ²⁷ D. M. T. Kuo and Y. C. Chang, 2018 IEEE 13th Nanotechnology Materials and Devices Conference.
 - ²⁸ M. Terraneo, M. Peyrard, and G. Casati, *Phys. Rev. Lett.* **88**, 094302 (2002).
 - ²⁹ B. W. Li, L. Wang, and G. Casati, *Phys. Rev. Lett.* **93**, 184301 (2004).
 - ³⁰ Y. Li, X. Y. Shen, Z. H. Wu, J. Y. Huang, Y. X. Chen, Y. S. Ni, and J. P. Huang, *Phys. Rev. Lett.* **115**, 195503 (2015).
 - ³¹ C. R. Otey, W. T. Lau, and S. H. Fan, *Phys. Rev. Lett.* **104**, 154301 (2010).
 - ³² D. H. He, S. Buyukdagli and B. Hu, *Phys. Rev. B* **80**, 104302 (2009).
 - ³³ B. Li, L. Wang, and G. Casati, *Appl. Phys. Lett.* **88**, 143501 (2006).
 - ³⁴ L. Wang and B. Li, *Phys. Rev. Lett.* **99**, 177208 (2007).